ACS APPLIED MATERIALS & INTERFACES

Research Article

www.acsami.org

Enhanced Performance of PTB7:$PC_{71}BM$ Solar Cells via Different Morphologies of Gold Nanoparticles

Annie Ng,[†] Wai Kin Yiu,[‡] Yishu Foo,[§] Qian Shen,[†] Amina Bejaoui,[§] Yiying Zhao,[†] Huseyin Cem Gokkaya,[†] Aleksandra B. Djurišić,[‡] Juan Antonio Zapien,[§] Wai Kin Chan,[∥] and Charles Surya*[,†]

[†]Department of Electronic and Information Engineering, The Hong Kong Polytechnic University, Hung Hom, Hong Kong

[‡]Department of Physics and [∥]Department of Chemistry, The University of Hong Kong, Pokfulam Road, Pok Fu Lam, Hong Kong

[§]Center of Super Diamond and Advanced Films (COSDAF) and Department of Physics and Materials Science, City University of Hong Kong, Tat Chee Avenue, Kowloon Tong, Hong Kong

Supporting Information

ABSTRACT: The effects of gold nanoparticles (AuNPs) incorporated in the hole transporting layer (HTL) of poly[[4,8-bis[(2-ethylhexyl)oxy] benzo[1,2-b:4,5-b′] dithiophene-2, 6-diyl] [3-fluoro-2-[(2-ethylhexy)carbonyl]thieno-[3,4-*b*]thiophened iyl]] (PTB7): [6,6]-phenyl C_{71} butyric acid methyl ester ($PC_{71}BM$) based solar cells are being systematically investigated in terms of the optical properties, electrical properties, and photovoltaic performance. The impacts of AuNPs on the optical response of the devices are modeled by finite-difference time-domain (FDTD) simulation. The size of the AuNPs used in this work is around 50−70 nm, so that 10−20 nm penetrated from the HTL into the active layer. We found that the power conversion efficiencies (PCEs) of the devices with AuNPs are significantly enhanced from 7.5%, for the control device, to 8.0%, 8.1%, and 8.2% for Au nanosphere-, nanorod-, and nanocube-incorporated devices, respectively. Among the photovoltaic parameters of the AuNP devices, the short circuit current density (J_{SC}) exhibits the largest improvement, which can be attributed to the improved optical properties of the devices. On the basis of the calculation results, the scattering cross section for the samples in the presence of AuNPs can be enhanced by a factor of $\sim 10^{10}-10^{13}$ and Au nanocubes exhibit superior scattering cross section compared to the Au nanospheres and nanorods with the same linear dimension. From the experimental impedance spectroscopy results, we found that the addition of AuNPs had little effect on the electrical properties of the device. The device performance is also found to be sensitive to the concentration and morphology of the AuNPs.

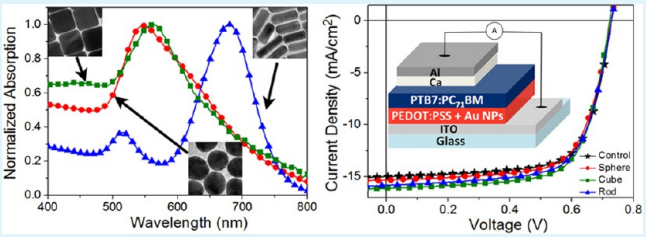

KEYWORDS: *polymer solar cells, gold nanoparticles, plasmonic effect, absorption, scattering, finite-difference time-domain*

1. INTRODUCTION

Sunlight, which is a clean, powerful, sustainable, and readily available energy source, is one of the potential alternatives to relieve the burden of our dependence on fossil fuels. Therefore, it is necessary to develop inexpensive solar cells able to efficiently convert solar energy into electricity. Organic solar cells, in particular polymer solar cells (PSCs), have attracted increasing attention owing to their unique properties such as low fabrication cost, light weight, and mechanical flexibility, allowing vacuum-free fabrication process and thin-film technology. These advantageous features of PSCs open up the opportunities for many novel applications.[1−5] However, PSCs are still suffering from low power conversion efficiency (PCE, η) compared to inorganic solar cells. Short exciton diffusion length, which is one of the major challenges of PSCs, limits the thickness of the active layer (<150 nm) resulting in poor light absorption and low J_{SC}.[6,7] Tremendous research efforts have been devoted to light trapping of the devices such as the application of diffraction gratings,[8−10] optical spacer layer,[9] microlenses,[11] and dielectric mirrors.[12,13] Recent studies indicate the incorporation of metallic NPs such as AuNPs and silver (Ag) NPs into the PSCs as a straightforward and efficient light trapping strategy.[14−23]

Numerous research groups have reported the significant enhancement of device performance by incorporating the metallic NPs into the hole transporting layer (HTL),[14−17] absorber layer (active layer),[18−21] or all layers of the devices.[22,23] When a metallic NP is stimulated by light, resonance is established when the frequency of incident electromagnetic field matches the frequency of the oscillating free electrons of the NP resulting in the free electrons oscillating coherently.[24] During the oscillation process, electrons are displaced relative to the nuclei and a force results from Coulomb attraction, causing the formation of various

Received: July 1, 2014
Accepted: November 19, 2014
Published: November 19, 2014

surface charge distributions in the nanostructure.[24,25] Each type of surface charge distribution can be characterized by a specific resonance frequency, which is also known as the localized surface plasmon resonance (LSPR). When an incident light with an appropriate frequency interacts with the NPs, its energy can be stored in the oscillation mode of the NPs resulting in absorption and/or scattering.[25] Au and Ag NPs are the choice of materials used for the purpose of light trapping since they have intense plasmonic resonances that lie within the UV−visible region of the solar spectrum which shift to lower frequencies with increasing NP sizes.[24,26] Depending on the dimensions, the metallic NPs can behave as the local field enhancers and/or light scatterers when incorporated into the solar cells so that the optical path can increase without changing the physical thickness of the absorber.[27−29] Other factors such as morphology, concentration, and the dielectric surrounding environment of the metallic NPs can also influence the plasmonic effect.[24] Numerous groups have compared the effects of size[17,19,23] and concentration[14,15,18,20] of the plasmonic NPs on the photovoltaic performances. There are also initial studies on incorporating different shapes of NPs, particularly nanospheres[16,17,19,22,23,30] and nanorods,[14,18,20] with PSCs while only a few studies focused on other morphologies.[15,21,31] Moreover, few detailed comparisons including both experiment and calculations are found in the literature on the effects of metallic NPs with different morphologies on the performances of the PSCs.[15] In addition, to the best of our knowledge, there has been no report on the study of the incorporation of Au nanocubes in PSCs.

In this paper, AuNPs with different morphologies (sphere, rod, and cube) were blended into the HTL layer, poly(3,4-ethylene-dioxythiophene):poly(styrenesulfonate) (PEDOT:PSS) before spin coating. The AuNPs chosen in this work are around 50−70 nm in dimension, which is in the range of the optimized size of NPs applied in PSCs.[17,19] The material system of PTB7:$PC_{71}BM$ is selected for this work as PTB7 is a promising low band gap polymer with extended light absorption spectrum and enhanced hole mobility compared to the conventional material system such as P3HT:$PC_{61}BM$.[32,33] We have compared the optical and electrical properties, as well as the photovoltaic performances, of the devices when employing AuNPs with different morphologies in PTB7:$PC_{71}BM$ based solar cells.

2. EXPERIMENTAL METHODS

2.1. Materials. Gold(III) chloride hydrate ($HAuCl_4$), silver nitrate ($AgNO_3$), cetyltrimethylammonium bromide (CTAB) were purchased from Sigma-Aldrich. Sodium borohydride ($NaBH_4$) and ascorbic acid were purchased from Acros Organic. Au nanospheres were purchased from EPRUI Nanoparticles and Micospheres Co. Ltd. PTB7 and $PC_{71}BM$ were purchased from 1-Material Inc. (Product OS0007; lotYY6142; M_w = 109 000 g/mol; PDI = 2.5) and Luminescence Technology Corp. (purity: >99.0%), respectively.

2.2. Preparation of Seed Solution. The procedures for the preparation of seed solution have been reported elsewhere.[34] The seed solution was obtained by adding 0.6 mL of ice-cold, freshly prepared 0.01 M $NaBH_4$ solution into a mixture composed of 0.25 mL of 0.01 M $HAuCl_4$ and 7.5 mL of 0.1 M CTAB. The solution was gently mixed until it turned yellow−brown, and was then kept in air at room temperature for at least 2 h before use.

2.3. Synthesis of Au Nanorods. The synthesis procedure for Au nanorods was reported in the literature.[35] Seed solution (10 μL) was added into the mixture composed of 2 mL of 0.01 M $HAuCl_4$, 0.4 mL of 0.01 M $AgNO_3$, 40 mL of 0.1 M CTAB, 0.32 mL of 0.1 M ascorbic acid, and 0.8 mL of 1.0 M HCl. After mixing gently for 10 s, the mixed solution was aged for 16 h at room temperature. Au nanorods were extracted by centrifugation. The obtained Au nanorods were then dispersed in deionized (DI) water.

2.4. Synthesis of Au Nanocubes. The detailed procedure for synthesis of Au nanocubes was previously reported.[34] A 0.2-mL portion of 0.01 M $HAuCl_4$ was added into a solution containing 8 mL of DI water and 1.6 mL of 0.1 M CTAB. The solution was gently mixed and then 0.95 mL of 0.1 M freshly prepared ascorbic acid and 5 μL of diluted Au seed solution were added. The prepared solution was placed in air for 15 min at room temperature. Finally, Au nanocubes were collected and dispersed in DI water after centrifugation. To enhance the batch-to-batch reproducibility of the AuNP suspension, the reaction solutions were prepared in large amount so that the mass of the extracted AuNPs could be weighed more accurately. In this work, we will conduct a systematic investigation on the impact of the shape of the AuNPs on the performance of the device with the concentration for all three types of AuNPs fixed at 31 mg/mL dispersed in DI water.

2.5. Device Fabrication. The blend solution preparation and device fabrication procedures, with the exception of the spin coating PEDOT:PSS process, were carried out in a nitrogen-filled glovebox with oxygen and moisture level lower than 0.1 ppm. PTB7:$PC_{71}BM$ blend solution, with a concentration of 25 mg/mL, was prepared by dissolving 10 mg of PTB7 and 15 mg of $PC_{71}BM$ in chlorobenzene/1,8-diiodoctane mixed solvent (97:3 vol %). The blended solution was stirred on a hot plate at 45 °C for at least 48 h and heated to 70 °C for 1 h before use. The device structure was indium tin oxide (ITO)/PEDOT:PSS/PTB7:$PC_{71}BM$/Ca (20 nm)/Al (100 nm), as illustrated in Figure 1. For the devices with AuNPs, optimized concentration of AuNPs suspension (3.5 vol % for Au nanospheres and nanocubes; 2.5 vol % for nanorods) was added into the PEDOT:PSS solution to obtain 1 mL of mixture, followed by mixing it in an ultrasonic bath for 1 h before use. The PEDOT:PSS solution with and without AuNPs (Clevios PVP Al4083) was passed through a 0.45-μm cellulose acetate membrane filter and spin-coated on cleaned substrates at 4000 rpm for 1 min followed by annealing at 130 °C for 20 min on a hot plate. The blend solution was then spin-coated on the PEDOT:PSS at 1500 rpm for 1 min. The samples were dried in the glovebox overnight and then methanol was spin-coated on the top of blend film at 2500 rpm for 40 s.[36] The electrode was deposited by thermal evaporation in a vacuum of ~10^{-8} Torr and the device area was 0.12 cm^2. The samples were encapsulated by a cover glass in the glovebox before taking out for characterization.

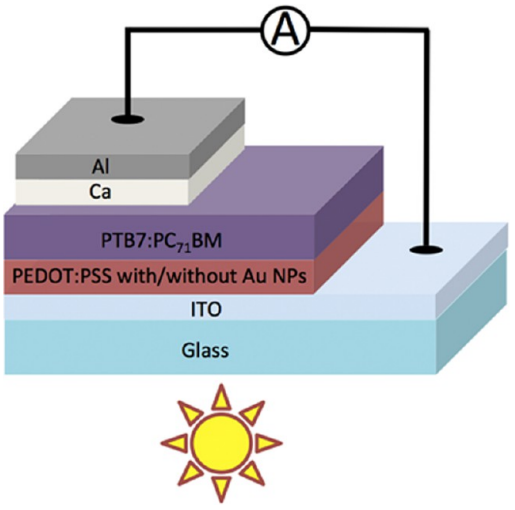

Figure 1. Device architecture of PTB7:$PC_{71}BM$ based solar cell.

2.6. Device Characterization. The $I-V$ characteristics of the solar cells were measured with a Keithley 2400 sourcemeter under AM 1.5 simulated sunlight illumination (ABET Technologies SUN 2000) at 100 mW/cm^2 determined by Molectron Power Max 500D laser

power meter. External quantum efficiency (EQE) was determined by a QE system from Enli Technology Co. Ltd. The EIS measurement was done by using a CH Instruments electrochemical workstation under 1 sun illumination. The surface morphologies of the PEDOT:PSS films were characterized by atomic force microscopy (AFM) in the tapping mode using a Bruker NanoScope 8. Reflectance of the samples in device structure was examined by using a PerkinElmer Lambda 750 UV/vis spectrometer equipped with an integrating sphere.

3. RESULTS AND DISCUSSION

The TEM images in Figure 2 show that the diameters of the commercial Au nanospheres and synthesized Au nanocubes are around 50 and 70 nm, respectively, while the length of the synthesized Au nanorods is around 70 nm with the diameter around 20 nm. This size range of the AuNPs can potentially enhance the light trapping of the devices by two approaches. First, the AuNP-induced LSPR effect can enhance the effective absorption cross-section by coupling the plasmonic near-field to the absorber layer,[28] which is possible for our case as the AuNPs partially penetrate (10−20 nm) from the HTL into the active layer. The AFM images for the PEDOT:PSS film containing AuNPs with different morphologies are shown in Figure 3, while the heights of the Au nanospheres, nanorods, and nanocubes penetrated from the HTL determined by the NanoScope Analysis software are shown in Supporting Information (SI) Figure S1. Second, the AuNPs can also act as light scatterers, which can increase the optical path lengths within the devices.[28] Under the condition of LSPR, the scattering cross-section will dramatically increase.[25] In this work, AuNPs incorporation into the HTL may induce the forward scattering and thus enhance the absorption capability of the absorber layer.

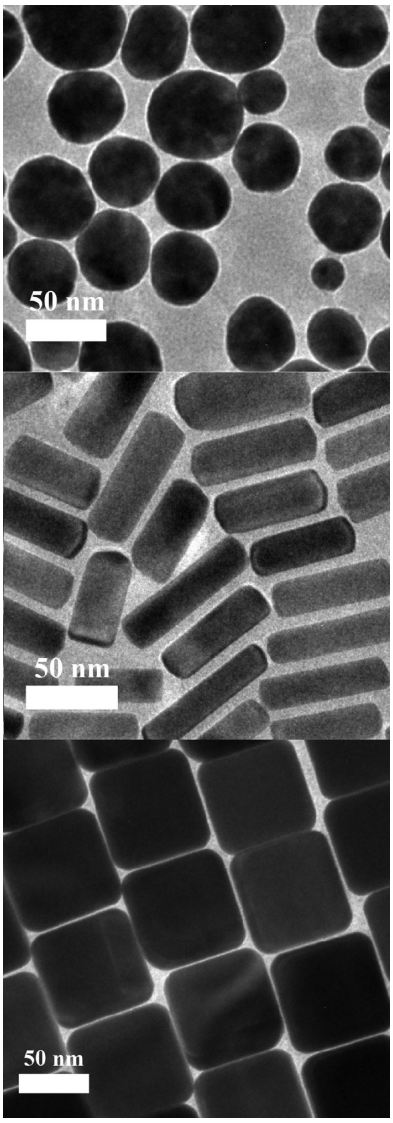

Figure 2. TEM images for AuNPs with different morphologies.

Different morphologies of AuNP exhibit distinct surface plasmon resonance peaks. Considering the fact that the excitation of surface plasmons can also be affected by the surrounding medium of AuNPs,[25] the films of PEDOT:PSS blended with AuNPs are prepared for measuring the absorption in order to obtain the results in the condition similar to the experiment. Figure 4 shows the UV−vis absorption spectra of the AuNPs with different morphologies blended in the film of PEDOT:PSS. The characteristic peaks are located at 540 and 560 nm for Au nanospheres and nanocubes, respectively. Two characteristic peaks, at 525 nm (transverse mode) and 680 nm (longitudinal mode), are observed for Au nanorods, which is due to the excitation of conduction electrons in the directions perpendicular and parallel to the length of the Au nanorods, respectively.[25] It is clearly observed from Figure 4 that all resonance peaks for AuNPs with different morphologies fall into the range of absorption spectrum of PTB7:$PC_{71}BM$, showing that the addition of these AuNPs into the PSCs can potentially enhance the light trapping of the devices by the LSPR effect.

Table 1 summarizes the photovoltaic parameters of devices with and without AuNPs and the corresponding $I-V$ curves are shown in Figure 5a. The devices with AuNPs included in Table 1 were fabricated under the optimized conditions. It is noted that the device performance is highly sensitive to the concentration of AuNPs blended into the HTL (see SI Figure S2). The FFs of the devices dropped significantly when the concentration of AuNPs increased to a higher volume percentage. In fact, exceedingly high density of AuNPs will easily lead to aggregation which will punch through the active layer and form undesired conducting paths between the ITO and the metal contact. The PCEs of the optimized AuNP devices have been enhanced by 2%−10%, of which, the devices with Au nanocubes show the largest improvements. To investigate the effects of AuNPs on solar cell performance, statistical analyses of the device parameters are given (see SI Figure S3). The devices with different AuNPs were fabricated in the same batch and can be compared fairly. The results show low variance among multiple devices with the same condition. The significant improvement in J_{SC} clearly reflects the trend of enhancement in light trapping of the devices by using AuNPs with different morphologies.

We then conducted detailed experiments in order to identify the underlying mechanism for the improvement in the PCE of the devices incorporating AuNPs, with consideration of the fact that the presence of metal back contact in a full device can reflect part of the incident light that passes through the active layer back into the device again thus increasing the effective optical path length between the AuNPs and the metal back contacts. Likewise, the presence of additional layers in the completed device offers opportunities for effects not present on single films such as wave guiding arising from enhanced scattering by the AuNPs. It is expected that the light trapping

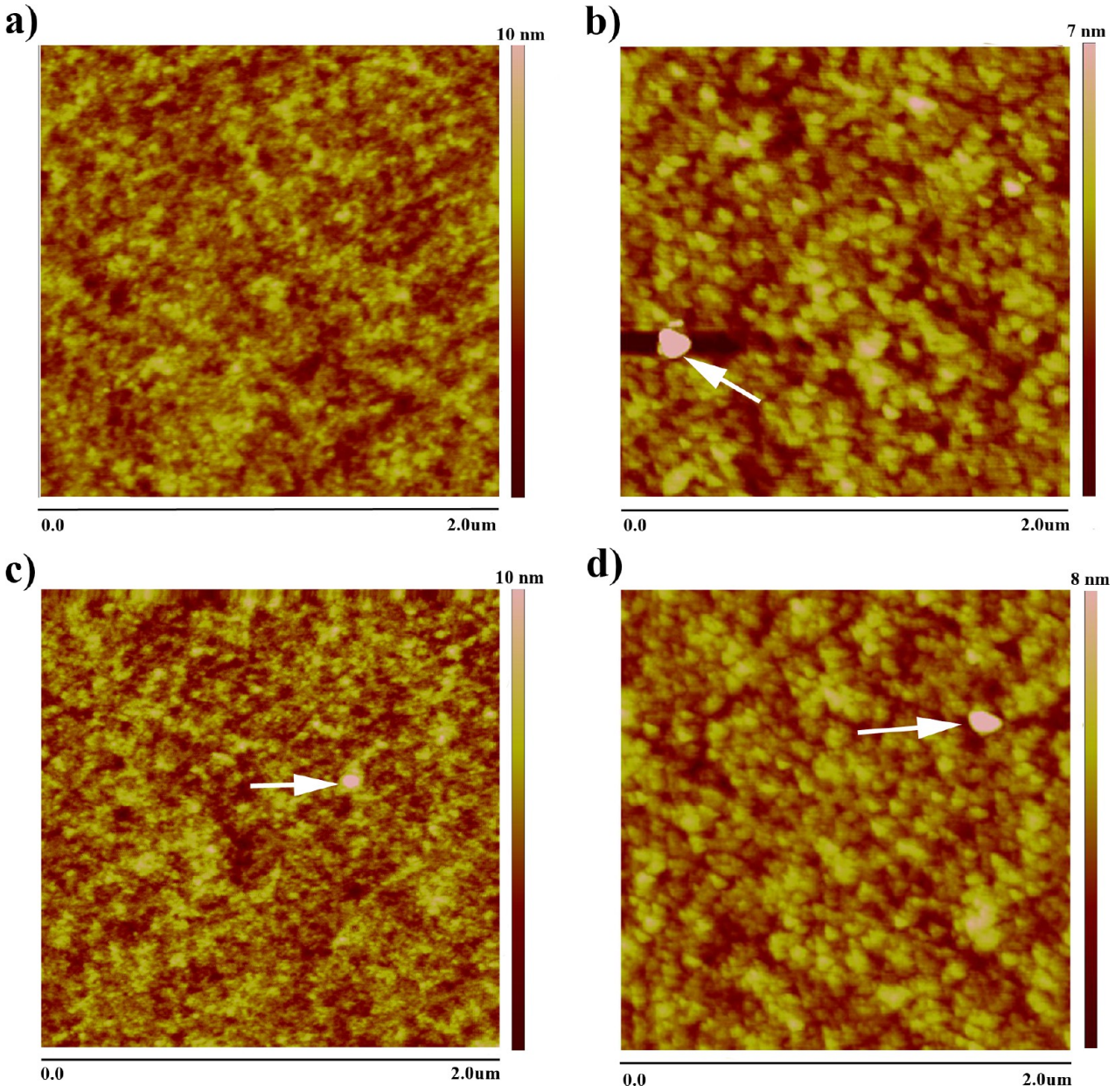

Figure 3. (a) Topography of AFM images for PEDOT:PSS without AuNPs (RMS: 0.9 nm), (b) with Au nanocubes (RMS: 1.0 nm), (c) with Au nanospheres (RMS: 1.0 nm), and (d) with Au nanorods (RMS: 0.9 nm).

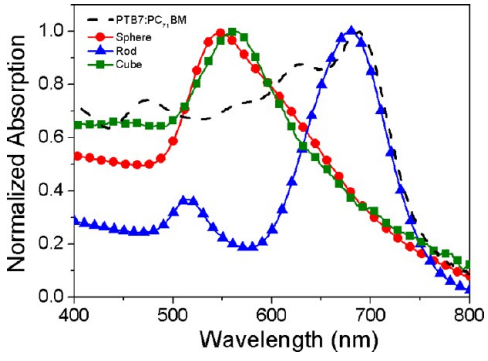

Figure 4. Normalized absorption spectra for PEDOT:PSS film blended with AuNPs and pure PTB7:$PC_{71}BM$.

ability can be substantially enhanced in the device structure.[37] Therefore, the impacts of the AuNPs on optical properties of the solar cells were investigated by measuring the reflectance from the back of the samples (ITO side) with the real device structure. The obtained results are shown in Figure 5b. In this study, lower reflectance of the sample indicates that more incident light can be trapped within the devices, which can potentially enhance the photon absorption efficiency of the active layer. It is clearly observed that all the devices incorporating AuNPs exhibit lower reflectance compared to the control device, except that the Au nanosphere device shows slightly higher reflectance from 500 to 570 nm compared to the others. Overall, the obtained trend of reflectance is $R_{control} > R_{sphere} > R_{rod} > R_{cube}$, which is in good agreement with the enhancement of device efficiency ($\Delta\eta_{cube} > \Delta\eta_{rod} > \Delta\eta_{sphere}$) as indicated in Table 1.The external quantum efficiency (EQE) of the devices was measured and the obtained spectra are plotted

dx.doi.org/10.1021/am504250w | ACS Appl. Mater. Interfaces 2014, 6, 20676−20684

Table 1. Photovoltaic Parameters Obtained for PTB7:$PC_{71}BM$ Solar Cells with or without AuNPs[a]

device		V_{oc} (V)	J_{sc} (mA/cm^2)	FF	η (%)	ΔPCE (%)	R_0 (Ωcm^2)	R_1 (Ωcm^2)	R_2 (Ωcm^2)
control	average	0.73 ± 0.01	15.1 ± 0.3 (15.3)	0.68 ± 0.02	7.5 ± 0.2		1.3	167	1365
sphere	average	0.73 ± 0.01	15.4 ± 0.2 (15.8)	0.68 ± 0.02	7.6 ± 0.2	2	1.4	129	1296
	best	0.73	15.6	0.70	8.0	7			
rod	average	0.73 ± 0.01	15.9 ± 0.2 (16.0)	0.67 ± 0.01	7.8 ± 0.2	4	1.3	122	1302
	best	0.73	15.9	0.70	8.1	8			
cube	average	0.73 ± 0.01	16.3 ± 0.2 (16.5)	0.67 ± 0.01	7.9 ± 0.2	6	1.4	112	1267
	best	0.73	16.7	0.68	8.2	10			

[a]The average values and errors of performance parameters were obtained from 12 devices. The J_{sc} values estimated from EQE are given in brackets.

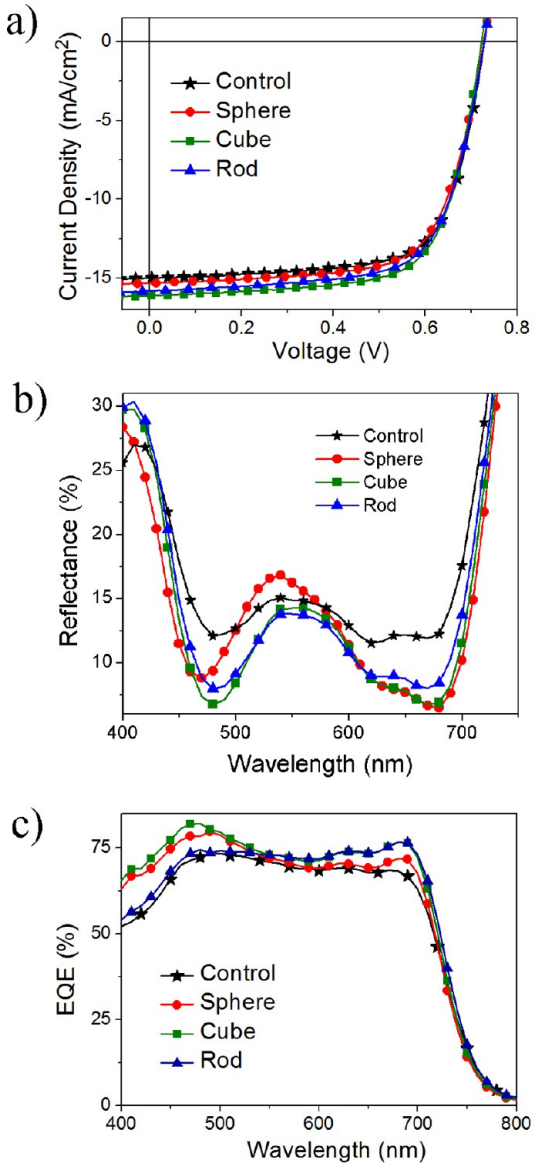

Figure 5. (a) *I*–*V* and (b) reflectance of the devices with different morphologies of AuNPs. (c) EQE curves of solar cells with different morphologies of AuNPs.

in Figure 5c. The integrated current density of the devices determined from the EQE indicated in Table 1 shows good agreement with the *I*–*V* results. Comparing Figure 5b and 5c, it is observed that EQE spectra are complementary to the reflectance spectra. The relatively less enhancement in EQE for AuNPs incorporated devices from 550 to 600 nm is likely due to the increase in the reflectance of the devices at the corresponding wavelengths. Besides, it is noticed that there is a valley at ∼475 nm and ∼670 nm for the reflectance spectra, which ideally would lead to a corresponding peak in EQE results, which are, in general, consistent with the observation from our experimental data. It is noteworthy that minor discrepancies are found between the reflectance and EQE results for the Au nanosphere and nanorod devices, which is not surprising since the reflectance data only illustrate the optical properties of the samples while the results of EQE can be affected by both optical and electrical properties. Moreover, the difference in equipment setup such as beam size should be also taken into account, particularly for the samples which are larger than the beam size. Therefore, the obtained EQE results may not be exactly the inverted version of reflectance spectra. Nevertheless, the experimental results above clearly indicate that enhancement in the photovoltaic performance is sensitive to the morphology of AuNPs incorporated in the devices, for which the Au nanocube devices exhibit the largest improvement in J_{SC} and PCE owing to the superior reduction in reflectance and enhancement in EQE over the broad visible light spectrum.

FDTD simulations have been carried out to further investigate the effect of AuNPs' morphology in terms of size and shape on the resulting optical characteristics. In general, the scattering cross sections of the AuNPs demonstrate significant dependence on the size of the NPs. Detailed FDTD simulations were performed to study photon scattering properties of AuNPs of varying sizes. The results demonstrate that the scattering cross sections of AuNPs increase substantially with the particle size (SI Figure S4) which may contribute to the enhancement of light trapping and the improvement in the device efficiency. It is noteworthy that the AuNPs need to be sufficiently close to the optimal size to be effective in enhancing the device performance because exceedingly small AuNPs will result in insignificant improvement; on the other hand, excessively large AuNPs may punch through the active layer, forming undesirable conducting paths between the ITO and metal electrodes. To investigate the effect of the morphology alone on the scattering rate, we have compared the scattering cross sections of the Au nanosphere and Au nanorod with that of the Au nanocube of comparable dimension. The simulated results on the scattering rate for AuNPs with the same linear dimension, cross sectional area, or volume are shown in Figure 6a. It is noteworthy that Au nanospheres are independent of the polarization of the incident electric field due to its symmetrical orientation in the medium, while Au nanocubes and nanorods exhibit anisotropic properties for which the orientations of AuNPs are highly sensitive to the polarization of the incident electric field. For the sake of simplicity, only 2 orientations for Au nanocubes and 2 orientations for Au nanorods have been considered during FDTD simulation (identified in the inset of Figure 6a). It is observed that the Au

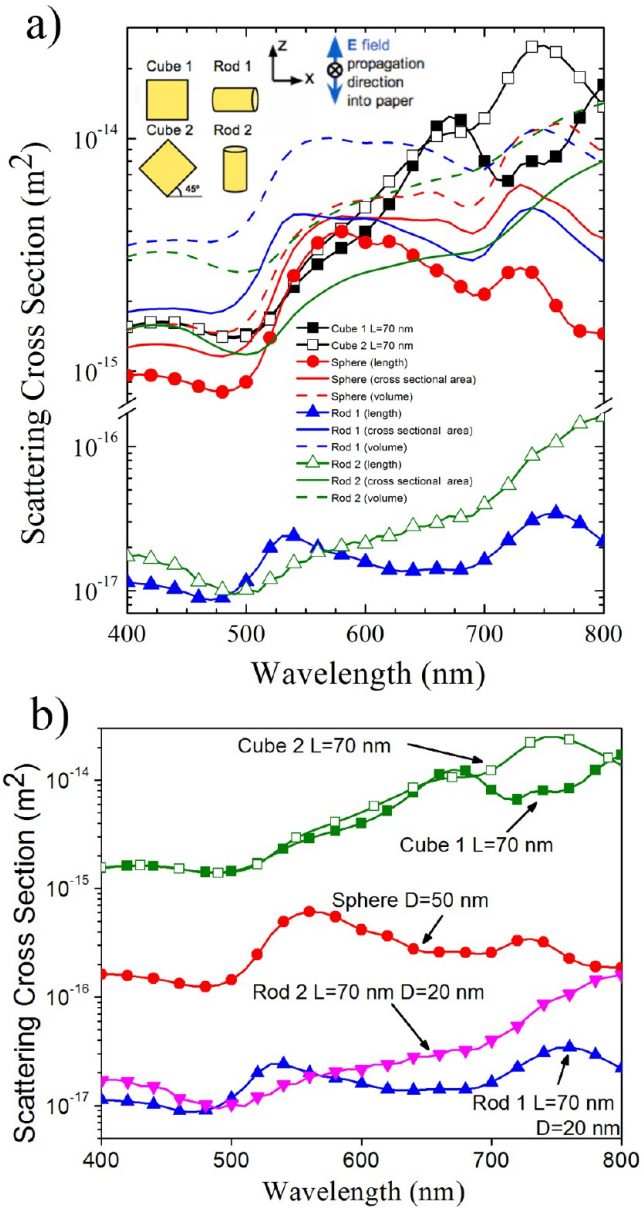

Figure 6. (a) Comparison of scattering cross section of Au nanocube (length 70 nm) with Au nanosphere and nanorod in terms of same linear dimension, same cross sectional area, and same volume (inset: the different orientations of nanocube and nanorod). (b) Scattering cross section for AuNPs with different morphologies. The sample without AuNPs is in the order of 10^{-27} (not shown in the graph).

nanocube exhibits the highest scattering cross section compared to the nanosphere and nanorod with the same linear dimension, which agrees with our expectation, as the cubic shape possess more sharp corners and larger surface contact area with the medium compared to the spherical and rod shape and thus Au nanocubes can exhibit stronger light trapping capability for the devices.[38] On the other hand, it is observed that the magnitudes of the scattering cross sections become comparable with each other for all three types of NPs with the same volume and cross sectional area. To verify experimentally whether the performance enhancement is dominated by the shape or size, we have fabricated additional devices, for which we compare the photovoltaic performance of the Au nanocube devices (40, 50, and 70 nm) with Au nanospheres (50 nm) and Au nanorods devices (L: 70 nm; D: 20 nm). It is noted that we choose the nanocubes with linear dimensions highly comparable with other type of AuNPs used in the experiment and aim to identify whether the enhancement effect is attributed to the change in the shape. The results are summarized in SI Table S1. It is observed that the J_{SC} decreases from 16.0 to 15.4 mA/cm^2 when the linear dimension of Au nanocubes is reduced from 70 to 40 nm, which is expected based on the results of scattering cross section with the variation in the linear dimension of particles as indicated in SI Figure S4. Nevertheless, based on the experimental results, the extent of enhancement for Au nanocube devices (7%−9%) with similar particle linear dimension compared to other shapes is substantially larger than that of nanorods (5%) and nanospheres devices (4%), confirming that the device performance is also sensitive to the shape of AuNPs used. For the incorporation of AuNPs in photovoltaic devices, Au nanocubes are preferred since they exhibit the highest scattering cross section for similar linear dimension compared to nanospheres and nanorods, leading to superior enhancement in J_{SC}.

We have also studied the scattering effect of AuNPs based on the current device geometry. Figure 6b shows the scattering cross section of AuNPs in the control design (without AuNPs) and in the presence of AuNPs partially embedded in PEDOT:PSS and the active layer. It is found that the scattering cross section for the sample without AuNPs is ∼10^{-27} m^2 while the sample in the presence of AuNPs is ∼10^{-17}−10^{-14} m^2 which is greatly enhanced by a factor of ∼10^{10}−10^{13}. The results clearly demonstrate that nanocubes show the strongest scattering effect, followed by nanospheres and then nanorods. Recent studies by Baek et al.[17] clearly indicate that plasmonic forward scattering is the dominant factor in the enhancement of EQE. Detailed FDTD simulation was performed to investigate the fraction of forward scattering for each type of AuNPs and the results are shown in SI Figure S5. From the data we observe that Au nanorods demonstrate the highest fraction for forward scattering relative to the total scattering among the three nanoparticles, which is followed by the nanocubes, while the nanospheres have the lowest fraction among the three. However, due to the small calculated scattering cross section of the nanorod, as shown in Figure 6b and SI Figure S4, we deduce that scattering by the nanorods will constitute relatively less contribution to the enhancement in EQE of the device and the improvement of the optical response from ∼600 to ∼700 nm is attributed to the strong plasmonic absorption at ∼680 nm which cannot be eliminated. Furthermore, it is clear that the superior light-trapping capability for nanocube device leading to significant enhancement in EQE and J_{SC} can be attributed to its large scattering cross section and high fraction for forward scattering as indicated in Figures 6b and SI S5, respectively. It is noteworthy that Figures 6b and SI S5 indicate that the advantage over the nanosphere is most substantial in the ranges ∼400 to ∼500 nm and ∼600 to ∼700 nm. This is consistent with the experimental data of reflectance and EQE as shown in Figure 5b and 5c. It is interesting to point out that the EQE data for the nanorod incorporated device indicates low EQE values between ∼400 and ∼500 nm, but for wavelength between ∼600 and ∼700 nm the EQE values of the device increase above that of the nanosphere incorporated device and are found to be comparable to those of the nanocube incorporated device. This result is contrary to the data presented in Figure 6b and SI Figure S5. To account for the discrepancy it is noted that the final EQE results are affected by

multiple factors including both plasmonic-enhanced absorption and scattering. Figure 4 clearly indicates a significant rise in the plasmonic absorption spectrum for the film blended with Au nanorods at wavelength between 600 to 700 nm. In contrast, for films blended with Au nanospheres and Au nanocubes a significant drop in the absorption spectra was observed within the same frequency range. This phenomenon should be also taken into account for the observed increase in the EQE from 600 to 700 nm for the Au nanorods devices.

Figure 7 demonstrates the electric field intensity enhancement for the sample with or without AuNPs, while the corresponding absorption per unit volume for the samples with or without AuNPs is given in SI Figure S6. We observed that the E-field enhancement for all types of AuNPs is strongly localized and near-field, while the scattering cross section is calculated based on the actual case as observed from AFM (1 AuNP in the area of 2 μm × 2 μm). Furthermore, the plasmonic-enhanced absorption is wavelength-dependent, which appears at the specific resonance frequency instead of entire spectrum while broadband enhancement can be achieved by the effect of scattering. Therefore, we believed that the plasmonic enhanced absorption would be limited to the vicinity of AuNPs and hence become less effective compared to optical scattering in our case. On the basis of the results obtained so far, we deduce that enhancements in device performance in the presence of AuNPs is possibly the combined effects of both plasmonic-enhanced absorption and light scattering, which are difficult to distinguish independently in this work.

Impedance spectroscopy (IS) is a useful technique capable of analyzing the resistive and capacitive contributions of different layers or interfaces to the electrical response of the entire device separately.[39] In this work we use IS to investigate the effects of AuNPs on the electrical properties of the fabricated devices; the resulting Nyquist plots are shown in Figure 8a while the equivalent circuit, which has been commonly used for modeling PSCs, is shown in Figure 8b.[40] The detailed interpretation of each circuit element in the equivalent circuit has been discussed in ref 39. Briefly, the resistance R_0 represents the resistive loss in the ITO and PEDOT:PSS while R_1 and R_2 represent the bulk resistance and recombination resistance, respectively.[40,41] The values of R_0, R_1, and R_2 of the devices with or with AuNPs are summarized in Table 1. It was found that the values of R_0 are similar among the devices with and without AuNPs, indicating that the addition of AuNPs into PEDOT:PSS does not significantly affect the resistance of ITO and PEDOT:PSS. This result is expected since the concentration of AuNPs blended in PEDOT:PSS is relatively low. Because of the low density of AuNPs, as confirmed by AFM images shown in Figure 3, the effect of Au on the reduction of R_0 is negligible despite the fact that Au is a conductive material. It is also found that the addition of AuNPs has a positive effect on reducing the bulk resistance of the devices. On the other hand, the recombination resistance of the devices with AuNPs is reduced. This result is also expected since the bare AuNPs are partially penetrated into the active layer, which may act as a recombination site for the charge carriers generated from the donor/acceptor interfaces. In fact, this shortcoming can be avoided by using Au@SiO_2 core/shell structure.[23] Thus, the reduction in the bulk resistance due to the introduction of AuNPs is compensated by increasing the probability of charge recombination in the active layer. Therefore, it was deduced that AuNPs added into the HTL have minor effect on the enhancement in the charge transport and collection; this result

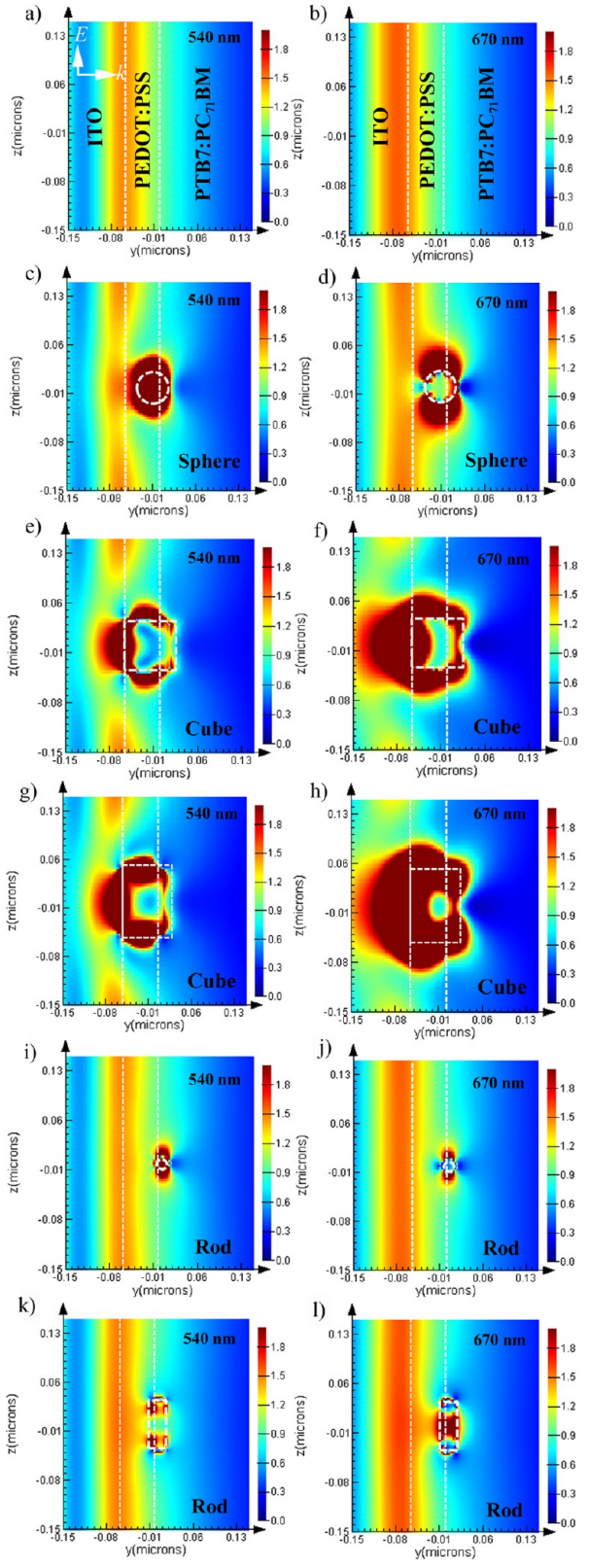

Figure 7. E-field intensity distribution of (a), (b) without AuNPs; (c), (d) sphere; (e), (f) cube with orientation 1; (g), (h) cube with orientation 2; (i), (j) rod with orientation 1 (the length is perpendicular to the incident E-field); and (k), (l) rod with orientation 2 (the length is parallel to the incident E-field) at wavelengths of 540 and 670 nm, respectively.

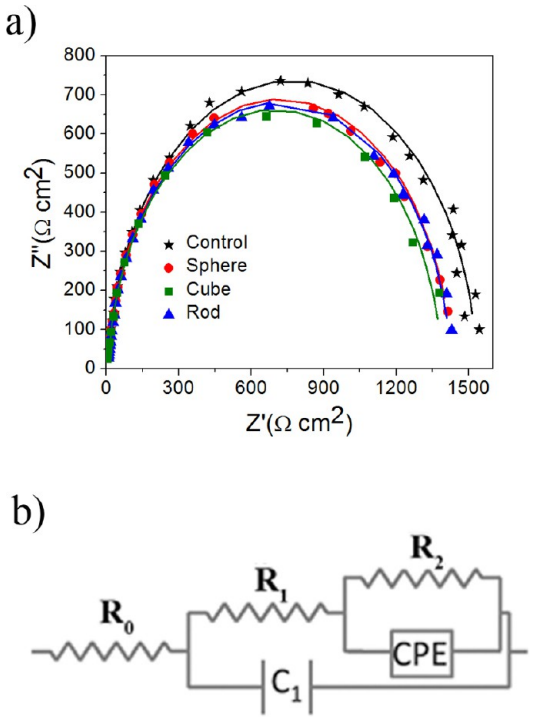

Figure 8. (a) Nyquist plots of solar cells with and without AuNPs. (b) The equivalent circuit used for data fitting.

is consistent with the observed small changes in FF with or without AuNPs as reported in Table 1.

4. CONCLUSION

We have performed a comprehensive study to investigate the effect of incorporating AuNPs into the HTL of PTB7:$PC_{71}BM$ based solar cells. It was found that the device performance is highly sensitive to the concentration and the morphologies of the AuNPs. Under the optimized conditions, around 2%−10% enhancement in device efficiency can be obtained by blending the AuNPs into the HTL of devices. The significant enhancement of the photovoltaic performance of the devices can be attributed to the advance optical properties of the AuNPs incorporated samples while the electrical response induced by the AuNPs has minor effect on the device efficiency. Among the three morphologies of AuNPs used in the experiment, the devices with Au nanocubes show the largest increase in PCE, which is due to the significant enhancement in absorption over the broad spectral region from 400 to 700 nm. Detailed FDTD simulation was performed to investigate the scattering for each type of AuNPs. Based on our calculations, Au nanocubes exhibit superior forward scattering power compared to the nanospheres and nanorods, suggesting that Au nanocubes are the preferable candidate for light trapping in photovoltaic devices.

■ ASSOCIATED CONTENT

Supporting Information

Height of NPs penetrating into the active layer determined from AFM, *I*−*V* characteristics of the devices for different AuNPs concentrations, scattering cross sections for samples with AuNPs with different sizes and morphologies, comparison of forward scattering of different shape of AuNPs, absorption per unit volume for different morphologies of AuNPs. Summary of photovoltaic performance for the devices with different linear dimension of Au nanocubes compared to nanospheres and nanorods. This material is available free of charge via the Internet at http://pubs.acs.org.

■ AUTHOR INFORMATION

Corresponding Author

* Tel: +852 2766 6220. Fax: +852 2362 8439. E-mail: charles.surya@polyu.edu.hk.

Notes

The authors declare no competing financial interest.

■ ACKNOWLEDGMENTS

This work was supported by the RGC Theme-based Research Scheme (Grant HKU T23-713/11). Partial support was provided by the RGC Collaborative Research Grant (Grant CUHK1/CRF/12G), and the Strategic Research Theme, University Development Fund, Seed Funding Grant of the University of Hong Kong. J.A.Z. acknowledges funding from GRF Project 122812 from the Research Grants Council of Hong Kong. We thank Dr. P. K. S. Shin and Mr. Billy K. Y. Kwan from the Department of Biology and Chemistry, City University of Hong Kong for assisting in measurement of reflectance.

■ REFERENCES

(1) Lipomi, D. J.; Tee, B. C. K.; Vosgueritchian, M.; Bao, Z. N. Stretchable Organic Solar Cells. *Adv. Mater.* **2011**, *23*, 1771−1775.
(2) Kim, J. Y.; Noh, S.; Lee, D.; Lee, C. Organic Tandem Solar Cell Using a Semi-transparent Top Electrode for Both-side Light Absorption. *J. Korean Phys. Soc.* **2010**, *57*, 1852−1855.
(3) Miyazaki, T.; Akisawa, A.; Kashiwagi, T. Energy Savings of Office Buildings by the Use of Semi-transparent Solar Cells for Windows. *Renewable Energy* **2005**, *30*, 281−304.
(4) Zhu, R.; Kumar, A.; Yang, Y. Polarizing Organic Photovoltaics. *Adv. Mater.* **2011**, *23*, 4193−4198.
(5) Park, H. J.; Xu, T.; Lee, J. Y.; Ledbetter, A.; Guo, L. J. Photonic Color Filters Integrated with Organic Solar Cells for Energy Harvesting. *ACS Nano* **2011**, *5*, 7055−7060.
(6) Brabec, C. J.; Sariciftci, N. S.; Hummelen, J. C. Plastic Solar Cells. *Adv. Funct. Mater.* **2001**, *11*, 15−26.
(7) Dennler, G.; Scharber, M. C.; Brabec, C. J. Polymer-Fullerene Bulk-Heterojunction Solar Cells. *Adv. Mater.* **2009**, *21*, 1323−1338.
(8) Na, S. I.; Kim, S. S.; Kwon, S. S.; Jo, J.; Kim, J.; Lee, T.; Kim, D. Y. Surface Relief Gratings on Poly(3-hexylthiophene) and Fullerene Blends for Efficient Organic Solar Cells. *Appl. Phys. Lett.* **2007**, *91*, 173509.
(9) Niggemann, M.; Riede, M.; Gombert, A.; Leo, K. Light Trapping in Organic Solar Cells. *Phys. Status Solidi A* **2008**, *205*, 2862−2874.
(10) Na, S. I.; Kim, S. S.; Jo, J.; Oh, S. H.; Kim, J.; Kim, D. Y. Efficient Polymer Solar Cells with Surface Relief Gratings Fabricated by Simple Soft Lithography. *Adv. Funct. Mater.* **2008**, *18*, 3956−3963.
(11) Tvingstedt, K.; Zilio, S. D.; Inganäs, O.; Tormen, M. Trapping Light with Micro Lenses in Thin Film Organic Photovoltaic Cells. *Opt. Express* **2008**, *16*, 21608−21615.
(12) Agrawal, M.; Peumans, P. Broadband Optical Absorption Enhancement through Coherent Light Trapping in Thin-film Photovoltaic Cells. *Opt. Express* **2008**, *16*, 5385−5396.
(13) Lunt, R. R.; Bulovic, V. Transparent, Near-infrared Organic Photovoltaic Solar Cells for Window and Energy-scavenging Applications. *Appl. Phys. Lett.* **2011**, *98*, 113305.
(14) Mahmound, A. Y.; Zhang, J.; Ma, D.; Izquierdo, R.; Truong, V. High Efficiency Polymer Solar Cells with Wet Deposited Plasmonic Gold Nanodots. *Org. Electron.* **2012**, *13*, 3102−3107.
(15) Kozanoglu, D.; Apaydin, D. H.; Cirpan, A.; Esenturk, E. N. Power Conversion Efficiency Enhancement of Organic Solar Cells by

Addition of Gold Nanostars, Nanorods, and Nanospheres. *Org. Electron.* **2013**, *14*, 1720−1727.
(16) Lu, L.; Luo, Z.; Xu, T.; Yu, L. Cooperative Plasmonic Effect of Ag and Au Nanoparticles on Enhancing Performance of Polymer Solar Cells. *Nano Lett.* **2013**, *13*, 59−64.
(17) Baek, S.; Noh, J.; Lee, C.; Kim, B.; Seo, M.; Lee, J. Plasmonic Forward Scattering Effect in Organic Solar Cells: A Powerful Optical Engineering Method. *Sci. Rep.* **2013**, *3*, 1726.
(18) Mahmound, A. Y.; Zhang, J.; Ma, D.; Izquierdo, R.; Truong, V. Thickness Dependent Enhanced Efficiency of Polymer Solar Cells with Gold Nanorods Embedded in the Photoactive Layer. *Sol. Energy Mater. Sol. Cells* **2013**, *116*, 1−8.
(19) Li, X.; Choy, W. C. H.; Huo, L.; Xie, F.; Sha, W. E. I.; Ding, B.; Guo, X.; Li, Y.; Hou, J.; You, J.; Yang, Y. Dual Plasmonic Nanostructures for High Performance Inverted Organic Solar Cells. *Adv. Mater.* **2012**, *24*, 3046−3052.
(20) Xu, X.; Kyaw, A. K. K.; Peng, B.; Zhao, D.; Wong, T. K. S.; Xiong, Q.; Sun, X. W.; Heeger, A. J. A Plasmonically Enhanced Polymer Solar Cell with Gold−silica Core−shell. *Org. Electron.* **2013**, *14*, 2360−2368.
(21) Wang, D. H.; Kim, D. Y.; Choi, K. W.; Seo, J. H.; Im, S. H.; Park, J. H.; Park, O. O.; Heeger, A. J. Enhancement of Donor−Acceptor Polymer Bulk Heterojunction Solar Cell Power Conversion Efficiencies by Addition of Au Nanoparticles. *Angew. Chem., Int. Ed.* **2011**, *50*, 5519−5523.
(22) Choi, H.; Lee, J.; Ko, S.; Jung, J.; Park, H.; Yoo, S.; Park, O.; Jeong, J.; Park, S.; Kim, J. Y. Multipositional Silica-Coated Silver Nanoparticles for High-Performance Polymer Solar Cells. *Nano Lett.* **2013**, *13*, 2204−2208.
(23) Chen, B.; Zhang, W.; Zhou, X.; Huang, X.; Zhao, X.; Wang, H.; Liu, M.; Lu, Y.; Yang, S. Surface Plasmon Enhancement of Polymer Solar Cells by Penetrating Au/SiO_2 Core/shell Nanoparticles into All Organic Layers. *Nano Energy* **2013**, *2*, 906−915.
(24) Kelly, K. L.; Coronado, E.; Zhao, L. L.; Schatz, G. C. The Optical Properties of Metal Nanoparticles: The Influence of Size, Shape, and Dielectric Environment. *J. Phys. Chem. B* **2003**, *107*, 668−677.
(25) Garcia, M. A. Surface Plasmons in Metallic Nanoparticles: Fundamentals and Applications. *J. Phys. D: Appl. Phys.* **2011**, *44*, 283001.
(26) Cole, J. R.; Halas, N. J. Optimized Plasmonic Nanoparticle Distributions for Solar Spectrum Harvesting. *Appl. Phys. Lett.* **2006**, *89*, 153120.
(27) Atwater, H. A.; Polman, A. Plasmonics for Improved Photovoltaic Devices. *Nat. Mater.* **2010**, *9*, 205−213.
(28) Stratakis, E.; Kymakis, E. Nanoparticle-based Plasmonic Organic Photovoltaic Devices. *Mater. Today* **2013**, *16*, 133−146.
(29) Gan, Q.; Bartoli, F. J.; Kafafi, Z. H. Plasmonic-Enhanced Organic Photovoltaics: Breaking the 10% Efficiency Barrier. *Adv. Mater.* **2013**, *25*, 2385−2396.
(30) Kalfagiannis, N.; Karagiannidis, P. G.; Pitsalidis, C.; Panagiotopoulos, N. T.; Gravalidis, C.; Kassavetis, S.; Patsalas, P.; Logothetidis, S. Plasmonic Silver Nanoparticles for Improved Organic Solar Cells. *Sol. Energy Mater. Sol. Cells* **2012**, *104*, 165−174.
(31) Stavytska-Barb, M.; Salvador, M.; Kulkarni, A.; Ginger, D. S.; Kelley, A. M. Plasmonic Enhancement of Raman Scattering from the Organic Solar Cell Material P3HT/PCBM by Triangular Silver Nanoprisms. *J. Phys. Chem. C* **2011**, *115*, 20788−20794.
(32) Liang, Y.; Yu, L. A New Class of Semiconducting Polymers for Bulk Heterojunction Solar Cells with Exceptionally High Performance. *Acc. Chem. Res.* **2010**, *43*, 1227−1236.
(33) Liang, Y.; Xu, Z.; Xia, J.; Tsai, S. T.; Wu, Y.; Li, G.; Ray, C.; Yu, L. For the Bright Future—Bulk Heterojunction Polymer Solar Cells with Power Conversion Efficiency of 7.4%. *Adv. Mater.* **2010**, *22*, E135−E138.
(34) Dovgolevsky, E.; Haick, H. Direct Observation of the Transition Point Between Quasi-Spherical and Cubic Nanoparticles in a Two-Step Seed-Mediated Growth Method. *Small* **2008**, *4*, 2059−2066.
(35) Ming, T.; Zhao, L.; Yang, Z.; Chen, H.; Sun, L.; Wang, J.; Yan, C. Strong Polarization Dependence of Plasmon-Enhanced Fluorescence on Single Gold Nanorods. *Nano Lett.* **2009**, *9*, 3896−3903.
(36) Zhou, H.; Zhang, Y.; Seifter, J.; Collins, S. D.; Luo, C.; Bazan, G. C.; Nguyen, T. Q.; Heeger, A. J. High-Efficiency Polymer Solar Cells Enhanced by Solvent Treatment. *Adv. Mater.* **2013**, *25*, 1646−1652.
(37) Fernández, S.; Bollero, A.; Naranjo, F. B.; de Abril, O.; Gandía, J. J. Optimization of ZnO:Al Based Back Reflectors for Applications in Thin Film Flexible Solar Cells. *Vacuum* **2014**, *99*, 56−61.
(38) Lu, X.; Rycenga, M.; Skrabalak, S. E.; Wiley, B.; Xia, Y. Chemical Synthesis of Novel Plasmonic Nanoparticles. *Annu. Rev. Phys. Chem.* **2009**, *60*, 167−192.
(39) Fabregat-Santiago, F.; Garcia-Belmonte, G.; Mora-Seró, I.; Bisquert, J. Characterization of Nanostructured Hybrid and Organic Solar Cells by Impedance Spectroscopy. *Phys. Chem. Chem. Phys.* **2011**, *13*, 9083−9118.
(40) Leever, B. J.; Bailey, C. A.; Mark, T. J.; Hersam, M. C.; Durstock, M. F. In Situ Characterization of Lifetime and Morphology in Operating Bulk Heterojunction Organic Photovoltaic Devices by Impedance Spectroscopy. *Adv. Energy Mater.* **2012**, *2*, 120−128.
(41) Guerrero, A.; Ripolles-Sanchis, T.; Boix, P. P.; Garcia-Belmonte, G. Series Resistance in Organic Bulk-Heterojunction Solar Devices: Modulating Carrier Transport with Fullerene Electron Traps. *Org. Electron.* **2012**, *13*, 2326−2332.